Table IV
Mössbauer Parameters[a]

species	δ, mm s^{-1}	ΔE_Q, mm s^{-1}	ref
PVP–heme 1a deoxy	0.95	2.06	this work
PVP–heme 1a carboxy	0.23	0.38	this work
PVP–heme 1a oxy	0.25	2.11	this work
Hb deoxy	0.91	2.26	25, 26
Hb carboxy	0.26[b]	0.26[b]	25, 26
Hb oxy	0.26	2.19	25, 26

[a] Values at 77 K. [b] Values at 4.2 K.

the oxygen-binding affinity of the heme analogous compounds in amide solvents such as dimethylformamide is enhanced in comparison with those in nonpolar solvents.[9,23] But in Table III one notices that the oxygen-binding affinity of the PVP-bound heme is smaller ($p_{50}(O_2)$ is larger) than that of the PVP-nonbound heme analogue. The smaller $k_{on}(O_2)$ value of the polymer-bound heme brings about the lower oxygen binding affinity (larger $p_{50}(O_2)$ value) in comparison with those of the nonbound analogue, and the resultant oxygen-binding affinity of the polymer-bound hemes resembles that of Hb in T state.

Mössbauer parameters, the isomer shift (δ) and quadrupole splitting (ΔE_Q), of the deoxy, carboxy, and oxy PVP–heme are summarized in Table IV with the reference data. For the deoxy PVP–heme, the δ value is larger than that for deoxy Hb, which suggests that the fixation of the imidazole ligand with spacer group and/or the surrounding polymer matrix causes the iron–imidazole bond to weaken. The Mössbauer parameters of the oxygen adduct also were measured for the PVP–heme. The parameters are comparable with those of oxy-Hb; this means that the iron ion in the oxygen adduct is in the ferric low-spin state also for the synthetic polymer-bound heme.

Acknowledgment. This work was partially supported by a Grant-in-Aid for Scientific Research on Priority Area "macromolecular complexes" and for Special Project Research on organometallic compounds from the Ministry of Education, Science and Culture, Japan.

Registry No. **2**, 9004-54-0; **3a′**, 96964-15-7; **3a′** ^{57}Fe derivative, 108919-00-2; **3b′**, 108918-99-6; CO, 630-08-0; O_2, 7782-44-7; protoporphyrin IX mono[*N*-(5-methylimidazol-1-yl)pentyl]amide mono(ethyl ester), 78897-43-5; 1-(5-aminopentyl)-2-methylimidazole, 78881-19-3; PVP-*co*-(4-aminostyrene), 79031-51-9; 4-aminostyrene, 1520-21-4; (4-aminophenyl)ethyl alcohol, 104-10-9; ethyl chloroformate, 541-41-3; dextran carbonate, 37359-17-4; ethylenediamine, 107-15-3; dextran amino derivative, 75301-70-1.

References and Notes

(1) Jones, R. D.; Summerville, D. A.; Basolo, F. *Chem. Rev.* **1979**, *79*, 139.
(2) Traylor, T. G. *Acc. Chem. Res.* **1981**, *14*, 102.
(3) Collman, J. P. *Acc. Chem. Res.* **1977**, *10*, 265.
(4) Shigehara, K.; Shinohara, K.; Sato, Y.; Tsuchida, E. *Macromolecules* **1981**, *14*, 1153.
(5) Tsuchida, E.; Nishide, H.; Yuasa, M.; Hasegawa, E.; Matsushita, Y. *J. Chem. Soc., Dalton Trans.* **1984**, 1147 and references therein.
(6) (a) Nishide, H.; Ohno, H.; Tsuchida, E. *Makromol. Chem., Rapid Commun.* **1981**, *2*, 55. (b) Tsuchida, E.; Nishide, H.; Yokoyama, H. *J. Chem. Soc., Dalton Trans.* **1984**, 2383.
(7) Tsuchida, E.; Nishide, H.; Sato, Y. *J. Chem. Soc., Chem. Commun.* **1981**, 556.
(8) Traylor, T. G.; Chang, C. K.; Geibel, J.; Berzinis, A.; Mincey, T. *J. Am. Chem. Soc.* **1979**, *101*, 6716.
(9) (a) Chang, C. K.; Traylor, T. G. *J. Am. Chem. Soc.* **1973**, *95*, 8475. (b) Chang, C. K.; Traylor, T. G. *Ibid.* **1973**, *95*, 8477. (c) Chang, C. K.; Traylor, T. G. *Proc. Natl. Acad. Sci. U.S.A.* **1975**, *72*, 1166.
(10) Tsuchida, E.; Nishide, H.; Sato, Y.; Kaneda, M. *Bull. Chem. Soc. Jpn.* **1982**, *55*, 1890.
(11) Sinyavskii, V. G. *Ukr. Khim. Zh. (Russ. Ed.)* **1960**, *32*, 489.
(12) Warburg, O.; Negelein, E. *Biochem. Z.* **1932**, *244*, 9.
(13) Kol'tsave, G. N.; Krylova, N. K.; Vasil've, A. E.; Ovsepyan, A. M.; Shimak, V. M.; Rozenberg, G. Y. *Zh. Obshch. Khim.* **1977**, *47*, 1177.
(14) Hayashi, A.; Suzuki, T.; Shin, M. *Biochim. Biophys. Acta* **1973**, *310*, 309.
(15) Gibson, Q. H. *J. Physiol. (London)* **1956**, *134*, 112.
(16) Antonini, E.; Brunori, M. *Hemoglobin and Myoglobin in their Reactions with Ligands*; North-Holland: Amsterdam, 1971.
(17) Tsuchida, E.; Nishide, H.; Ohno, H. *J. Inorg. Biochem.* **1982**, *17*, 283.
(18) Allcock, H. R.; Neenan, T. X.; Boso, B. *Inorg. Chem.* **1985**, *24*, 2656.
(19) Bayer, E.; Holtzbach, G. *Angew. Chem., Int. Ed. Engl.* **1977**, *16*, 117.
(20) Traylor, T. G.; Berzinis, A. P. *Proc. Natl. Acad. Sci. U.S.A.* **1980**, *77*, 3171.
(21) Sharma, V. S.; Schmidt, M. R.; Ranny, H. M. *J. Biol. Chem.*, **1976**, *251*, 4267.
(22) Steinmeier, R. C.; Parkhurst, L. J. *Biochemistry* **1975**, *14*, 1564.
(23) Sawicki, C. A.; Gibson, Q. H. *J. Biol. Chem.* **1977**, *252*, 7538.
(24) Bringar, W. S.; Chang, C. K.; Geibel, J.; Traylor, T. G. *J. Am. Chem. Soc.* **1974**, *96*, 5597.
(25) Spartalian, K.; Lang, G.; Yonetani, T. *Biochim. Biophys. Acta* **1976**, *428*, 281.
(26) Lang, G.; Marshall, W. *Proc. Natl. Acad. Sci. U.S.A.* **1966**, *87*, 3.

Chain Dimensions in Deformed Networks: Theory and Comparison with Experiment

Burak Erman

School of Engineering, Bogazici University, Bebek 80815, Istanbul, Turkey.
Received December 29, 1986

ABSTRACT: Expressions for the transformation of the mean-squared chain vector and of the mean-squared radius of gyration in a deformed network are obtained according to the constrained junction model of rubber elasticity. Differences between the behavior of chain vectors and radii of gyration are indicated. Dependence of the state of microscopic deformation on the type of macroscopic strain, network chain length, junction functionality, and the extent of dilation during cross-linking is investigated. The microscopic state of strain is described completely in terms of the material parameters κ and ζ of the constrained junction model. Predictions of the theory are compared with results of small-angle neutron-scattering experiments reported by various investigators. Experimentally observed deviations of chain dimensions from those expected from the phantom and affine network models are explained with the present theory.

Introduction

The state of strain at the molecular level in a deformed network in equilibrium differs from the externally applied macroscopic state of strain. Recent results of neutron-scattering experiments on various polymeric networks show that the transformation of chain dimensions is significantly

0024-9297/87/2220-1917$01.50/0

less than the transformation of macroscopic dimensions.[1-7] These experiments indicate that the deviation of the microscopic state of deformation from the macroscopic one depends predominantly on (i) the molecular constitution of the network, such as chain type, chain length, and junction functionality, (ii) amount of solvent during cross-linking, and (iii) the type of imposed state of strain, such as uniaxial extension or isotropic swelling.

Various attempts have been made to describe the experimentally observed transformation of chain dimensions in terms of molecular models. In the simplest treatment,[8] based on the affine network model, each unit of the chain was assumed to transform affinely with macroscopic strain. Calculations of the transformation of the radii of gyration of chains in a phantom network were presented by Pearson[9] and others.[10-13] The microscopic state of strain obtained according to the affine and phantom network models constitutes the upper and lower limit, respectively, to the state of strain in a real network. However, neutron-scattering experiments showed evidence of microscopic transformations which were below those obtained from the phantom network model.[1,5,6] These observations led Bastide and colaborators to postulate the network unfolding hypothesis.[14] According to this hypothesis, topological rearrangements at a scale larger than that of the network mesh size cause a reduction in chain dimensions in the deformed network. The hypothesis was further incorporated into the molecular theory in more quantitative terms.[15]

The theoretical studies cited in the preceding paragraph investigate the effect of macroscopic deformation on the transformations of the mean-squared radius of gyration of network chains. The microscopic state of strain may alternatively be analyzed in terms of the transformation of the mean-squared end-to-end chain vector, which is related to but is different than the transformation of the mean-squared radius of gyration. Birefringence[16,17] and segmental orientation[18,19] in deformed networks have recently been analyzed in terms of the transformations of the mean-squared chain vectors.

In the present paper, microscopic state of deformation is formulated according to the constrained junction model of networks.[20,21] In the following section, transformations of the mean-squared end-to-end vector and the mean-squared radius of gyration are calculated and related to network constitution, to conditions of network preparation, and to the macroscopic state of strain. In order to afford comparison with results of neutron-scattering experiments, greater emphasis is placed on the calculation of the mean-squared radius of gyration. Detailed calculations of transformation of the end-to-end vectors can be found in previous work.[16] In the second section, predictions of the theory are compared with results of small-angle neutron-scattering experiments on deformed networks.

Theory

Transformation of the Mean-Squared End-to-End Vectors. The instantaneous end-to-end vector $\mathbf{r}$ for a chain of a network at equilibrium under a fixed strain may be expressed as

$$\mathbf{r} = \lambda \bar{\mathbf{r}}_{ph,0} + \Delta \mathbf{r} \tag{1}$$

where $\bar{\mathbf{r}}_{ph,0}$ is the time-averaged mean vector in the undeformed phantom network and $\Delta\mathbf{r}$ is the instantaneous fluctuation of $\mathbf{r}$ from the phantom mean. λ is the macroscopic displacement gradient tensor. When expressed in terms of principal coordinates, λ is diagonal. Each term represents the ratio of the final length along a principal direction to the corresponding reference length obtained during cross-linking. Accordingly, λ may be expressed as

$$\lambda = (v_{20}/v_2)^{1/3}\begin{bmatrix} \alpha_x & 0 & 0 \\ 0 & \alpha_y & 0 \\ 0 & 0 & \alpha_z \end{bmatrix} \tag{2}$$

Here, v_{20} and v_2 are the volume fractions of polymer during cross-linking and during experiment, respectively. α_x etc. represent the ratio of the final length to the corresponding length in the swollen but undistorted network. Thus α_x, α_y, and α_z reflect the degree of distortion of the network. Experimental evidence shows that the network as a closed system is approximately incompressible, and $\alpha_x\alpha_y\alpha_z = 1$. The determinant of λ defined by eq 2 is proportional to $v_{20}^{1/3}$. This proportionality forms the basis of network unfolding arguments to be presented more quantitatively in the following paragraphs.

The x component of eq 1 may be written as

$$x = \lambda_x \bar{x}_{ph,0} + \Delta x \tag{1'}$$

where the subscript 0 identifies dimensions in the reference state. The first term in eq 1 indicates that mean chain dimensions in a phantom network transform affinely with macroscopic deformation. According to theory, the component Δx representing fluctuations from the phantom mean depends on macroscopic deformation in a nonaffine manner. In the phantom model limit, Δx is independent of macroscopic deformation and $\Delta x = \Delta x_0$. In the affine limit, $\Delta x = \lambda_x \Delta x_0$. For a real network, Δx lies between the two limits, depending on the degree of constraints operating on chains.

Mean-squared values of x, $\bar{x}$, and Δx appearing in eq 1' are related by

$$\langle x^2 \rangle = \lambda_x^2 \langle \bar{x}_{ph}^2 \rangle_0 + \langle (\Delta x)^2 \rangle \tag{3}$$

In a phantom network, $\langle \bar{x}_{ph}^2 \rangle_0$ and $\langle (\Delta x)_{ph}^2 \rangle$ are related to $\langle x^2 \rangle_0$ by[22]

$$\langle \bar{x}^2 \rangle_0 = (1 - 2/\varphi)\langle x^2 \rangle_0$$
$$\langle (\Delta x)_{ph}^2 \rangle = (2/\varphi)\langle x^2 \rangle_0 \tag{4}$$

where φ is the average junction functionality. Using eq 4 in eq 3, one obtains

$$\langle x^2 \rangle = \left[(1 - 2/\varphi)\lambda_x^2 + (2/\varphi)\frac{\langle (\Delta x)^2 \rangle}{\langle (\Delta x)_{ph}^2 \rangle} \right] \langle x^2 \rangle_0 \tag{5}$$

Similar expressions hold for the y and z components of the mean-squared chain length.

Equation 5 formally relates the mean-squared end-to-end length of network chains in the deformed state to that in the undeformed state. In the previous treatment of chain dimensions,[16] the ratio appearing in brackets in eq 5 is expressed as

$$\frac{\langle (\Delta x)^2 \rangle}{\langle (\Delta x)_{ph}^2 \rangle} = \frac{\langle (\Delta X)^2 \rangle}{\langle (\Delta X)_{ph}^2 \rangle} = 1 + B_x \tag{6}$$

where $\langle (\Delta X)^2 \rangle$ and $\langle (\Delta X_{ph})^2 \rangle$ denote the mean-squared fluctuation of junctions from their average locations in the real and phantom networks, respectively. The term B_x is given according to the theory as

$$B_x = (\lambda_x - 1)(\lambda_x + 1 - \zeta\lambda_x^2)/(1 + g_x)^2 \tag{7}$$

with

$$g_x = \lambda_x^2[\kappa^{-1} + \zeta(\lambda_x - 1)] \tag{8}$$

The parameter κ in eq 8 represents the degree of constraints operating on junctions. It is assumed to be proportional to the number of junctions in the volume per-

vaded by a network chain.[23] In terms of molecular parameters, κ is expressed as[23]

$$\kappa = I\langle r^2\rangle_0^{3/2}(\mu/V^0)$$

$$\kappa = I(2/\varphi)(N_A d_0)(\langle r^2\rangle_0/M)^{3/2}M_c^{1/2}v_{20} \qquad (9)$$

where I is the constant of proportionality, N_A is Avogadro's number, d_0 is the density of dry polymer, M is the molecular weight of a chain of mean-squared length $\langle r^2\rangle_0$, (μ/V^0) is the cross-link density in the reference volume V^0, and M_c is the molecular weight between cross-links. Dependence of κ on functionality is included in the second part of eq 9. Experimental results on tetrafunctional networks[23] lead to a value of approximately $^1/_2$ for I.

The parameter ζ appearing in eq 7 and 8 is introduced to account for the nonaffine transformations of constraint domains surrounding junctions. In the original theory introduced by Flory,[20] the domains of constraint were assumed to transform affinely with macroscopic strain. Further work and comparison with experimental evidence revealed that nonhomogeneities in structure resulting in unequal compliances of chains emanating from a junction should produce a nonaffine component in the strain field of the constraint domains. The instantaneous displacement $\Delta\mathbf{s}$ of a junction from the location of the center of action of entanglement constraints was therefore assumed to consist of two components,

$$\Delta\mathbf{s} = \Delta\mathbf{s}' + \Delta\mathbf{s}''$$

where, $\Delta\mathbf{s}'$ and $\Delta\mathbf{s}''$ are the affinely and nonaffinely transforming components, respectively. Assuming that $\Delta\mathbf{s}'$ and $\Delta\mathbf{s}''$ are statistically uncorrelated, a transformation rule was assigned[21] to $\Delta\mathbf{s}$ as

$$\langle(\Delta s_x)^2\rangle = \lambda_x^2\langle(\Delta s'_x)^2\rangle_0 + \lambda_x^3\langle(\Delta s''_x)^2\rangle_0 \qquad (10)$$

with similar expressions for the y and z components. Denoting the mean-squared x component of the fluctuation of a junction in a phantom network by $\langle(\Delta X)^2\rangle$, the parameters κ and ζ are defined[21] as

$$\kappa = \langle(\Delta X)^2\rangle/\langle(\Delta s_x)^2\rangle_0 \qquad \zeta = \langle(\Delta s''_x)^2\rangle_0/\langle(\Delta X)^2\rangle \quad (11)$$

The ζ parameter is thus a measure of the nonaffine contribution to the deformation of constraint domains. Comparison of eq 10 and 11 sets a lower and an upper bound to ζ as

$$0 \leq \zeta \leq \kappa^{-1} \qquad (12)$$

Substitution of eq 6 in eq 5 leads to the x component of the molecular deformation tensor

$$\Lambda_x^2 = \langle x^2\rangle/\langle x^2\rangle_0 = (1 - 2/\varphi)\lambda_x^2 + (2/\varphi)(1 + B_x) \qquad (13)$$

Similar relations hold for the y and z components.

Results of sample calculations for uniaxial elongation along the x-axis ($\alpha_x = \alpha$, $\alpha_y = \alpha_z = \alpha^{-1/2}$) are presented in Figure 1 for a dry sample ($v_2 = 1$) cross-linked in the bulk ($v_{20} = 1$). The macroscopic elongation ratio, α, is plotted along the abscissa. Components of the molecular deformation tensor parallel and perpendicular to the direction of stretch are shown along the ordinate by $\Lambda_\parallel$ and $\Lambda_\perp$, respectively. The dashed curves represent results of calculations for the affine ($\kappa = \infty$) and phantom ($\kappa = 0$) network models. Calculations for a real network with $\kappa = 5$ and $\zeta = 0$ and 0.2 are shown by the solid curves. The solid curves for $\Lambda_\parallel$ converge to the phantom network result at high values of α not included in the figure. Convergence is much slower for the perpendicular component of the molecular deformation tensor. Increasing ζ decreases the parallel component. $\Lambda_\perp$ is not affected significantly by ζ. Unlike $\Lambda_\parallel$, $\Lambda_\perp$ remains close to the affine limit within the interval of α shown.

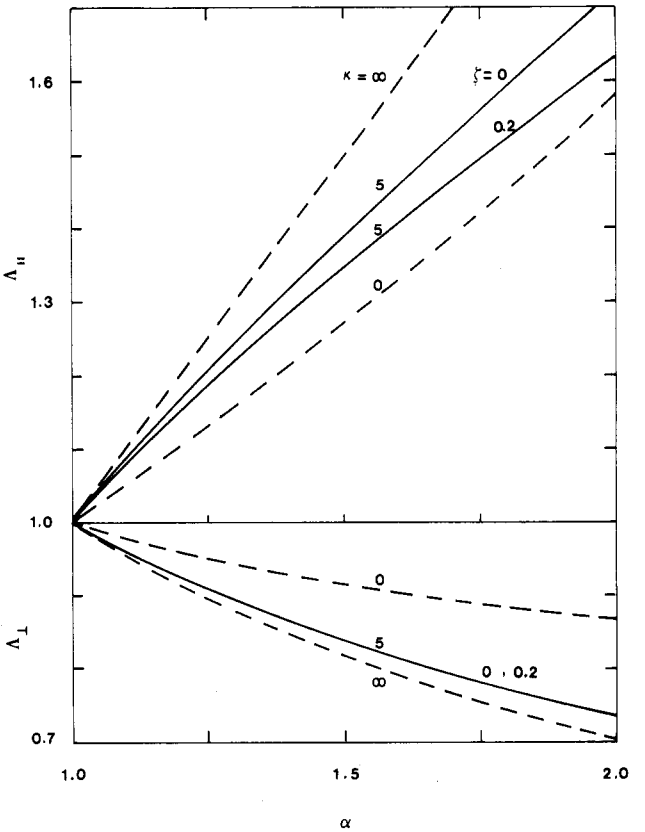

Figure 1. Transformation of root-mean-squared chain vectors, in directions parallel and perpendicular to the direction of stretch in uniaxial extension, α. Dashed curves show results for an affine and a phantom network model. Solid curves are for a real network with material parameters as identified.

Transformation of the Mean-Squared Radius of Gyration. The vector $\mathbf{r}_{ij}$ joining the ith and jth skeletal atoms of a network chain may be written as the sum of a phantom mean, $\bar{\mathbf{r}}_{ij,ph}$, and an instantaneous fluctuation, $\Delta\mathbf{r}_{ij}$, from this mean. Following Pearson,[9] the phantom mean may be assumed to transform affinely with macroscopic deformation. The mean-squared x component of $\mathbf{r}_{ij}$ may then be obtained as

$$\langle x_{ij}^2\rangle = \lambda_x^2\langle\bar{x}_{ij}^2\rangle_{0,ph} + \langle(\Delta x_{ij})^2\rangle \qquad (3')$$

According to the approach adopted by Pearson, the following relations exist between $\langle x_{ij}^2\rangle$, $\langle\bar{x}_{ij}^2\rangle$, and $\langle(\Delta x_{ij})^2\rangle$:

$$\langle\bar{x}_{ij}^2\rangle_0 = (1 - 2/\varphi)\eta^2\langle x^2\rangle_0$$

$$\langle(\Delta x_{ij})^2\rangle_0 = [\eta - (1 - 2/\varphi)\eta^2]\langle x^2\rangle_0 \qquad (14)$$

where

$$\eta = |i - j|/n \qquad (15)$$

and n is the number of segments in the network chain. For a phantom network, the mean-squared fluctuation $\langle(\Delta x_{ij})^2\rangle$ is independent of macroscopic strain. For a real network, however, it is a function of macroscopic strain depending on the degree of entanglements operating on the sequence. Substituting eq 14 in eq 3′ leads to

$$\langle x_{ij}^2\rangle = \left[(1 - 2/\varphi)\lambda_x^2\eta^2 + \frac{\langle(\Delta x_{ij}^2)\rangle}{\langle(\Delta x_{ij}^2)_{ph}\rangle}[\eta - (1 - 2/\varphi)\eta^2]\right]\langle x^2\rangle_0 \qquad (16)$$

The strain dependence of the fluctuation of the sequence is contained in the ratio $\langle(\Delta x_{ij})^2\rangle/\langle(\Delta x_{ij})_{ph}^2\rangle$ of eq 16.

When $|i - j| = n$, this ratio equates to $1 + B_x$ in accordance with eq 6. For shorter sequences, this ratio is expected to depart from $1 + B_x$, however. The degree of constraints on the end-to-end chain vector in a network is assumed to be proportional to the number of junctions in the volume occupied by the chain, as expressed by the first of eq 9. The degree of entanglement of a sequence ij may similarly be assumed to be proportional to the number of junctions present in the volume pervaded by the sequence. Adopting this assumption, the entanglement parameter κ_{ij} may be introduced for the sequence ij, in analogy with eq 9, as

$$\kappa_{ij} = I\langle r_{ij}^2\rangle_0^{3/2}(\mu/V^0) \tag{17}$$

where I is the constant of proportionality and $\langle r_{ij}^2\rangle$ is the mean-squared end-to-end distance for the sequence. The parameter κ_{ij} introduced in this manner reduces to κ of eq 9 for the whole chain ($|i - j| = n$) if the constant of proportionality in eq 17 is identified with that in eq 9. Introducing the ratio[9] η into eq 17, κ_{ij} may be related to κ by

$$\kappa_{ij} = \eta^{3/2}\kappa \tag{18}$$

For a network with $\langle r^2\rangle_0 = 70$ Å, there are ca. 40 junctions in the domain of a chain.[22] Accordingly, one junction is contained in a volume with a radius of 20 Å. Sequences whose mean-squared lengths are below 20 Å should therefore be relatively free of constraints imposed by junctions, and κ_{ij} for this sequence should equate to zero. For a chain with a characteristic ratio of 5 and segment length of 1.53 Å, the number of segments in such a sequence is 34, corresponding to $\eta = 0.08$. For sequences with η below this value, phantom network conditions will obtain. This lower limit is approximated by $\eta = 0$ in the following calculations.

As a first approximation, the ratio $\langle(\Delta x_{ij})^2\rangle\langle(\Delta x_{ij})^2\rangle_{ph}$ appearing in eq 16 may be replaced by an average

$$\frac{\langle(\Delta x_{ij})^2\rangle}{\langle(\Delta x_{ij})_{ph}^2\rangle} = 1 + \bar{B}_x \tag{19}$$

where

$$\bar{B}_x = \int_0^1 B_{x,ij}\,d\eta \tag{20}$$

$B_{x,ij}$ is given by eq 7 in which κ is replaced by κ_{ij} of eq 18. Substituting from eq 7, 8, and 18 into eq 20 leads to

$$\bar{B}_x = (\lambda_x - 1)(1 + \lambda_x - \zeta\lambda_x^2)\int_0^1 \frac{\eta^3\,d\eta}{(a + b\eta^{3/2})} \tag{21}$$

where

$$a = \lambda_x^2/\kappa \qquad b = 1 + \zeta\lambda_x^2(\lambda_x - 1) \tag{22}$$

Performing the integration in eq 21 leads to

$$\bar{B}_x = (\lambda_x - 1)(1 + \lambda_x - \zeta\lambda_x^2)\left[\frac{5a + 3b}{3b^2(a + b)} - \frac{10a^{2/3}}{9b^{8/3}}\left[\frac{3^{1/2}\pi}{6} - \frac{1}{2}\ln\frac{(1 + \psi)^2}{1 + \psi + \psi^2} + 3^{1/2}\arctan\frac{2 - \psi}{3^{1/2}\psi}\right]\right] \tag{23}$$

where $\psi = (a/b)^{1/3}$.

Replacing the ratio $\langle(\Delta x_{ij})^2\rangle/\langle(\Delta x_{ij})_{ph}^2\rangle$ in eq 16 with its preaveraged equivalent $1 + \bar{B}_x$ given by eq 23 and summing[9] over i and $j > i$ leads to the mean-squared radius of gyration of a chain in the deformed network.

$$\langle s_x^2\rangle = n^{-2}\sum_{j>i}\langle x_{ij}^2\rangle = [(1/2 - 1/\varphi)\lambda_x^2 + (1/\varphi + 1/2)(1 + \bar{B}_x)]\langle s_x^2\rangle_0 \tag{24}$$

where $\langle s_x^2\rangle_0 = \langle x^2\rangle_0/6$ in the Gaussian approximation. Dividing both sides of eq 24 by $\langle s_x^2\rangle_0$ leads to the x component of the deformation tensor Λ_g^2 for the radius of gyration. In general, for $t = x$, y, or z,

$$\Lambda_{g,t}^2 = \frac{\langle s_t^2\rangle}{\langle s_t^2\rangle_0} = (1/2 - 1/\varphi)\lambda_t^2 + (1/\varphi + 1/2)(1 + \bar{B}_t) \tag{25}$$

where $\langle s^2\rangle_0$ is the mean-squared radius of gyration in the state of reference obtained during cross-linking. By definition, the reference state corresponds to the minimum of the elastic free energy when $\lambda_t = 1$. Substituting $\lambda_t = 1$ into eq 25 shows that $\Lambda_{g,t}^2 = 1$ in the state of reference. In the dry state of the network which is cross-linked in solution, the components $\Lambda_{g,t}^2$ will be less than unity.

In the presentation of experimental data, the dry state of a network is customarily adopted as the reference state. This leads to an "apparent" molecular deformation tensor whose components $\Lambda_{g,t,app}^2$ are

$$\Lambda_{g,t,app}^2 = \langle s_t^2\rangle/\langle s_t^2\rangle_{dry} = \Lambda_{g,t}^2(\upsilon_{20},\upsilon_2,\alpha)/\Lambda_{g,t}^2(\upsilon_{20},1,1) \tag{26}$$

where the subscript dry refers to chain dimensions in the dry network. The numerator and the denominator of the second line of eq 26 are obtained from eq 25 with proper identification of the variables in parentheses.

In the limit of the phantom network model, $\kappa = \zeta = 0$. Substitution in eq 23 gives $\bar{B}_t = 0$, and eq 25 reduces to

$$\Lambda_{g,t}^2 = (1/2 - 1/\varphi)\lambda_t^2 + 1/\varphi + 1/2$$

in agreement with previous results of Pearson.[6,9] In the affine limit, $\kappa = \infty$, $\zeta = 0$. From eq 25, $\bar{B}_t = \lambda_t^2 - 1$, and

$$\Lambda_{g,t}^2 = \lambda_t^2$$

which is also in agreement with previous theory. The approximation introduced by preaveraging $\langle(\Delta x_{ij})^2\rangle/\langle(\Delta x_{ij})^2\rangle_{ph}$ in eq 16 leads to results which are in satisfactory agreement with experimental data as will be shown in the following section.

Results of calculations for $\Lambda_{g,t}^2$ based on eq 25 are shown in Figure 2 for uniaxial extension. Following the notation of experimental literature, components of Λ_g^2 along x (parallel to direction of stretch) and y (perpendicular to direction of stretch) directions are represented by $\Lambda_{g,\parallel}^2$ and $\Lambda_{g,\perp}^2$, respectively. The square roots of these variables are shown along the ordinate of Figure 2. The abscissa denotes the extension ratio α. Calculations are shown for the affine ($\kappa = \infty$) and phantom ($\kappa = 0$) network models and for a real network with $\kappa = 5$ and $\zeta = 0$ and 0.2 as identified in the figure. Results for $\kappa = 5$ converge to the phantom limit with increasing strain. $\Lambda_{g,\parallel}$ values for a network with $\kappa = 5$ are much closer to the phantom network values. Deviation of the solid curve for $\Lambda_{g,\perp}$ from the phantom network result is significant, however. Values of $\Lambda_{g,\perp}$ are not significantly affected by ζ while $\Lambda_{g,\parallel}$ values fall closer to the phantom limit with increasing ζ. Previous stress–strain experiments[23] on bulk cured tetrafunctional PDMS networks indicate that the value of $\kappa = 5$ corresponds approximately to a network with $M_c = 8000$. That the behavior of such a network along the direction of stretch is close to that of the phantom network has been estab-

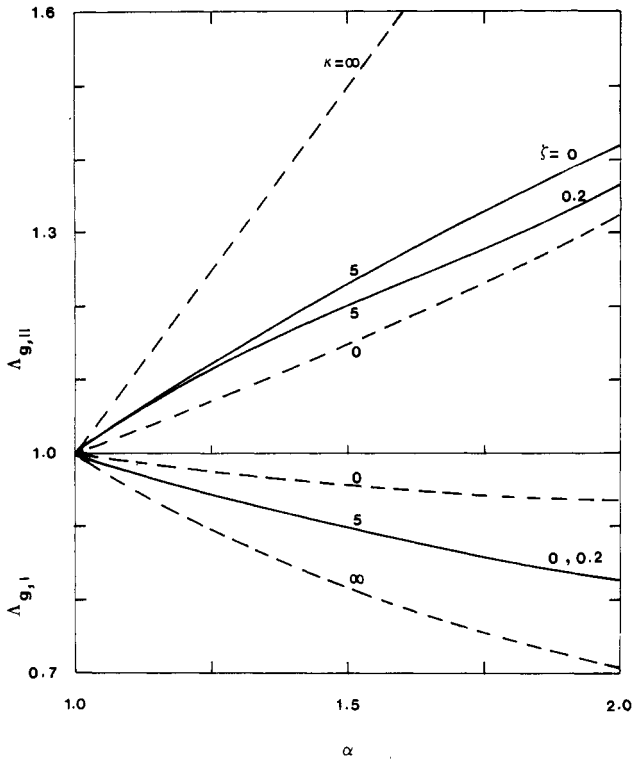

Figure 2. Transformation of root-mean-squared radius of gyration with macroscopic extension. See legend to Figure 1.

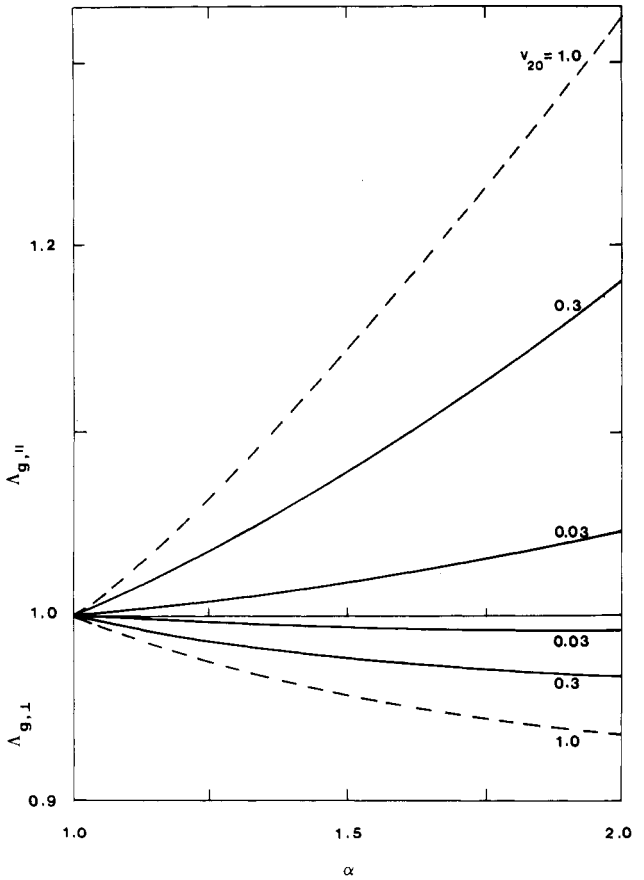

Figure 3. Effect of degree of dilution, v_{20}, during cross-linking on the microscopic state of strain in uniaxial extension.

lished by neutron-scattering experiments reported in the following section.

Dependence of Λ_g^2 on the degree of dilution during cross-linking is shown in Figure 3. Values of $\Lambda_{g,\parallel}$ and $\Lambda_{g,\perp}$ calculated by using eq 25 are normalized according to eq

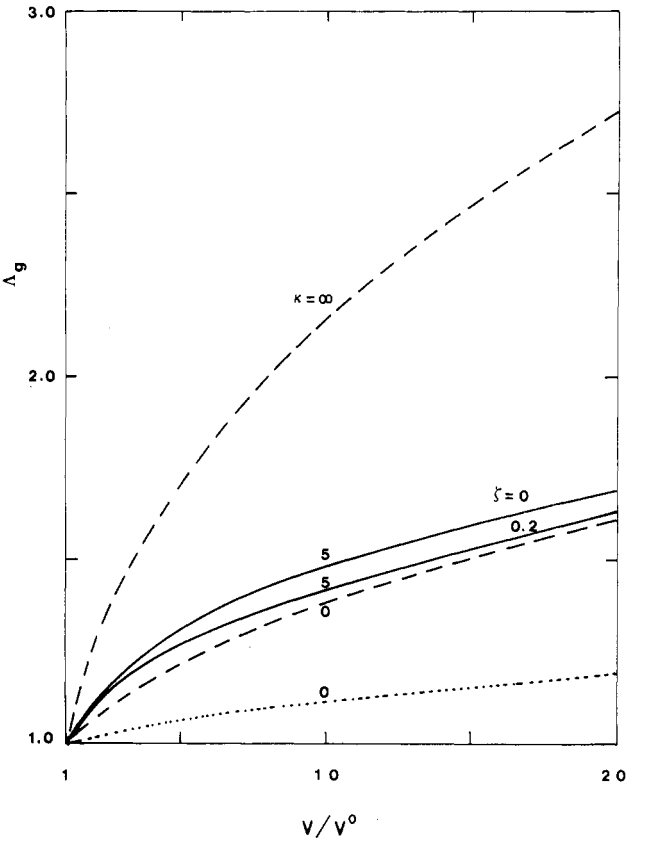

Figure 4. Effect of isotropic swelling, V/V^0, on the microscopic state of strain. Dashed curves are for the phantom and the affine network models. Solid curves are for real networks. The dotted curve is for a phantom network cross-linked at v_{20} = 0.1.

26. Results are given only for the phantom network. Further discussion for real networks is given in the final section of this paper. The dashed curves correspond to a network cross-linked in the bulk. Values of $\Lambda_{g,\parallel}$ and $\Lambda_{g,\perp}$ are observed to diminish significantly with increasing v_{20}.

The effect of isotropic swelling on chain dimensions is shown in Figure 4. Values of Λ_g are shown along the ordinate. The ratio of the final swollen volume V of network to volume V^0 during cross-linking is shown along the abscissa. The dashed curves represent results for the affine and the phantom limits. The solid curves for κ = 5 and ζ = 0 and 0.2 calculated for v_{20} = 1 lie very close to the phantom limit. The dotted curve is calculated for a phantom network prepared at v_{20} = 0.1. Values of Λ_g plotted along the ordinate are normalized according to eq 26.

Experiment

Comparison with Results of Small-Angle Neutron-Scattering Experiments. Results of small-angle neutron-scattering experiments[7] on uniaxially stretched polyisoprene networks are shown in Figure 5. The networks were prepared in the bulk with trifunctional end-linking. Circles and triangles represent experimental data. Values of $\Lambda_{g,\parallel}$ and $\Lambda_{g,\perp}$ are plotted as functions of extension ratio α. Dashed curves represent results of calculations based on the affine and phantom network models. Experimental data are seen to be subject to significant scatter. However, two trends in the data are clearly seen: Almost all of the points lie in the region between the phantom and affine limits, and $\Lambda_{g,\parallel}$ values are closer to the phantom limit, whereas $\Lambda_{g,\perp}$ values are closer to the affine limit. The solid curves represent results of calculations according to eq 25, with κ = 10 and ζ = 0.06. These values of κ and ζ were chosen to obtain the optimum agreement with ex-

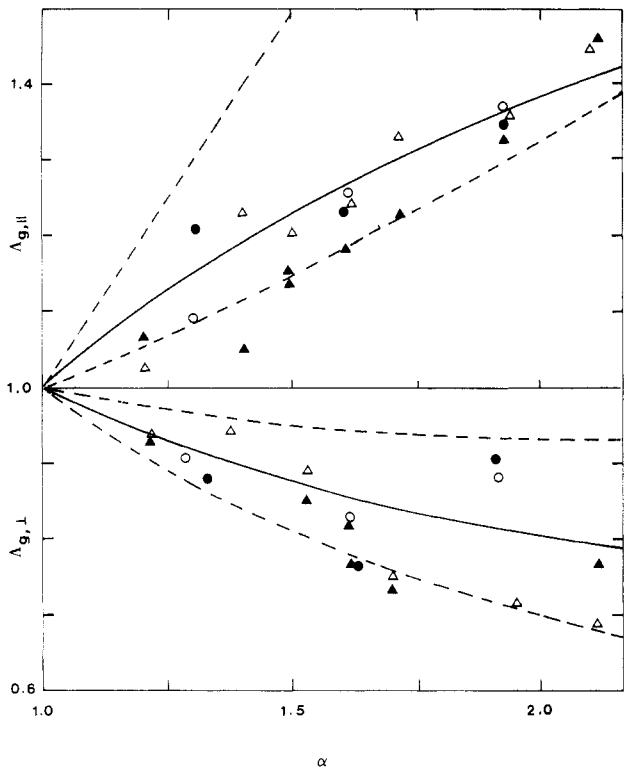

Figure 5. Transformation of the radius of gyration as a function of uniaxial extension of polyisoprene networks.[7] Circles and triangles represent experimental data for networks with different M_c and different amounts of deuteriated chains. Dashed curves are obtained for an affine and a phantom network. Solid curves represent results of the theory for a real network.

periment for the parallel and perpendicular components simultaneously. Values of υ_{20} and φ were set equal to 1 and 3, respectively. The chosen value of κ corresponds to a molecular weight M_c of (2–3) × 10^4 from eq 9. This range of values for M_c is less than the reported values of 2.9 × 10^4 and 6.4 × 10^4 of ref 7. Increasing κ to account for the larger values of M_c would move the theoretical curves closer to the affine limit. This would improve the agreement between theory and experiment for $\Lambda_{g,\parallel}$ but not for $\Lambda_{g,\perp}$.

Results of scattering experiments from isotropically swollen polystyrene gels are presented in Figure 6. The samples were prepared in solution (υ_{20} = 0.091) with M_c = 26 000 and with φ = 4. The data presented in Figure 6 correspond to sample A of ref 5. The ordinate values of the circles shown in Figure 6 are obtained by dividing the reported value of the radius of gyration in the swollen state by the corresponding value in the dry state. Corresponding calculations of Λ_g from eq 25, normalized according to eq 26, are shown by the solid curve. Material parameters are chosen as κ = 1, ζ = 0, υ_{20} = 0.091, and φ = 4. the value of κ = 1 is calculated from eq 9 for the polystyrene network with M_c = 26 000.

Results of experiments on PDMS networks[6] are presented in Figure 7. The circles represent experimental data. Curves are obtained by using eq 25 and 26. Filled circles represent results on bulk cured PDMS with φ = 4 and M_c = 10 000. Corresponding curves are obtained with κ = 1, ζ = 0.025, and υ_{20} = 0.9. Choice of the latter value instead of unity is based on the correction for the extracted amount of unreacted material reported in ref 6. Use of eq 9 for PDMS would give κ = 4–5 for this network which is higher than the value required for best fit. Empty circles represent data for PDMS networks cross-linked in the diluted state, with υ_{20} = 0.71. The average junction

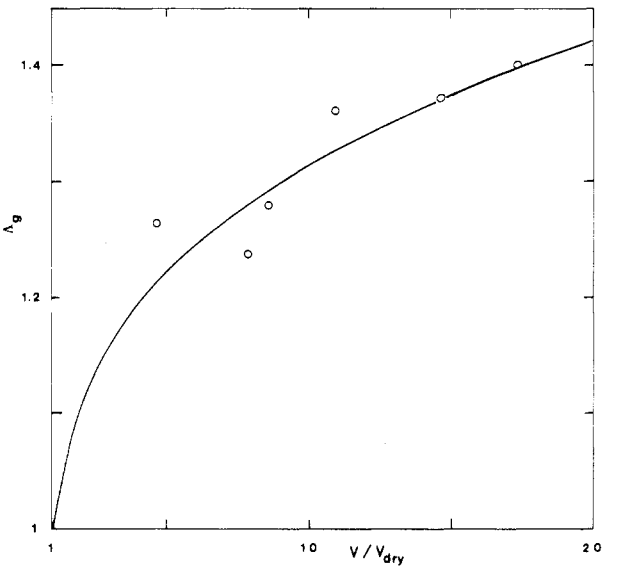

Figure 6. Transformation of the radius of gyration as a function of isotropic swelling of polystyrene networks.[5] Circles represent experimental data. The solid curve is obtained from the theory.

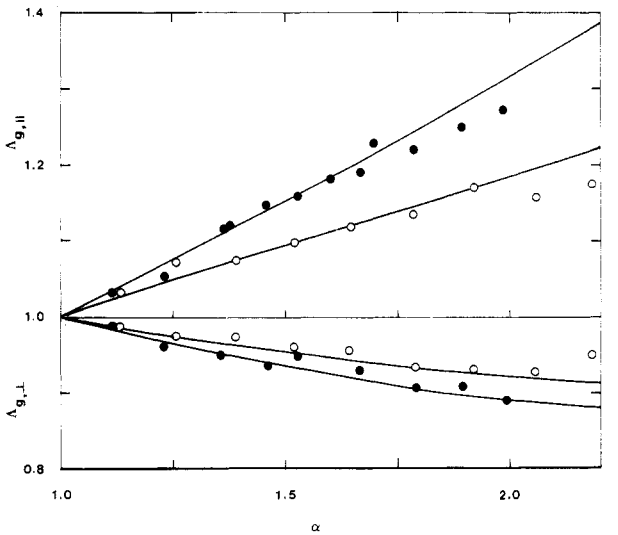

Figure 7. Transformation of the radius of gyration as a function of uniaxial extension of poly(dimethylsiloxane) PDMS networks.[6] Filled and open circles represent data for samples cross-linked in the bulk and in the diluted state, respectively. Curves are obtained by the theory.

functionality is reported as 3.1. This value was obtained[6] after correction for unreacted species. Consideration of unreacted sample should also lower the value of υ_{20} below 0.71. A value of υ_{20} = 0.50 (corresponding to 70% of the reported value) is assumed in the present calculations. Results are shown by the curves through the empty circles obtained with κ = 0.6 and ζ = 0.025. Use of eq 9 would give κ = 2.8 for this network which is again higher than the value chosen for best fit. If the discrepancy between the theoretical and experimental values of κ is disregarded, the results of calculations seem to agree satisfactorily with neutron-scattering results both in parallel and perpendicular directions.

Conclusion and Discussion

The deformation tensors Λ^2 and Λ_g^2 are two measures of the microscopic state of strain in a deformed network. The basic difference between the two tensors is that they yield information on the average transformations of different length scales in the network. Λ^2 is obtained by considering the transformation of the distance between the

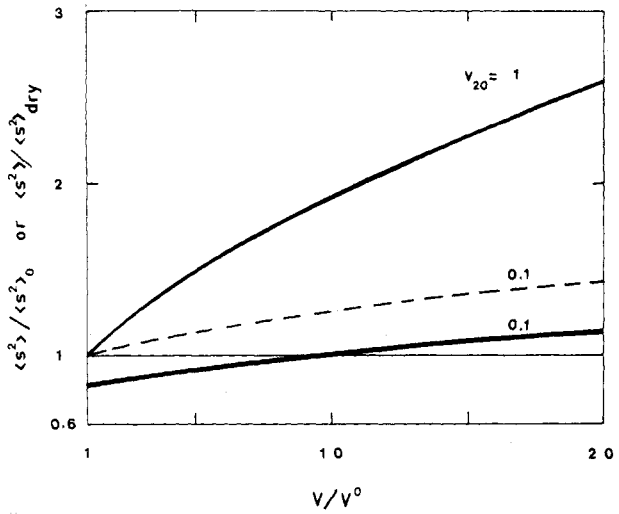

Figure 8. Results of calculations for transformation of the mean-squared radius of gyration with isotropic dilution. The upper curve represents $\langle s^2\rangle/\langle s^2\rangle_0$ for a network cross-linked in the bulk. The lower solid curve represents the same ratio for a network cross-linked at $v_{20} = 0.1$. $\langle s^2\rangle_0$ is the mean-squared radius of gyration in the state of cross-linking. The dashed curve shows results of calculations for $\langle s^2\rangle/\langle s^2\rangle_{dry}$ for a network cross-linked at $v_{20} = 0.1$. $\langle s^2\rangle_{dry}$ represents the mean-squared radius of gyration of chains in the dry undeformed state.

terminal pair of skeletal atoms of the chain, whereas Λ_g^2 is based on the transformation of the distances between all pairs of skeletal atoms. Comparison of Figures 1 and 2 shows that at a given macroscopic extension the mean-squared radius of gyration transforms less than the mean-squared chain vector. Components of Λ_g^2 are formulated on the assumption that the strength of constraints operating on a sequence is proportional to the number of cross-links present in the space pervaded by the sequence. This assumption affords the means to relate the microscopic transformations of the radius of gyration to the constitution of real networks.

The present theory and experimental data show that the degree of dilution during cross-linking and the extent of molecular interpenetration are the two dominant parameters affecting microscopic strain. The effect of v_{20} on the transformation of the radius of gyration is further illustrated in Figure 8. The dependence of $\langle s^2\rangle/\langle s^2\rangle_0$ on the isotropic degree of swelling, V/V^0, is presented for the phantom network by the solid curves. The upper solid curve is for a network cross-linked in the bulk. The lower solid curve is for cross-linking in solution at $v_{20} = 0.1$. The chains in this network are in a state of compression when $V/V^0 < 10$, as will be seen from the figure. Comparison of the two solid curves clearly shows the effect of the conditions during cross-linking on microscopic deformation. The dashed curve represents the ratio $\langle s^2\rangle/\langle s^2\rangle_{dry}$ for the network cross-linked in the bulk. $\langle s^2\rangle_{dry}$ is the mean-squared radius of gyration in the dry, bulk state. The curve shows that when $V/V^0 = 20$, $\langle s^2\rangle$ is 1.43 times larger than $\langle s^2\rangle_{dry}$. The upper curve shows that this ratio is 2.59. Reduction of the state of microscopic strain by increasing v_{20} is in agreement with the network unfolding hypothesis. This reduction becomes more pronounced in real networks for which κ is not zero but is given by eq 9. Analysis of Figures 1–4 shows that nonzero values of ζ further reduce the state of microscopic strain.

The present theoretical analysis is based on the assumption that the segment density is uniformly distributed during cross-linking at any given v_{20}. The linear dependence of κ on v_{20} results from this assumption.[24] High degrees of dilution during cross-linking may, however, result in nonhomogeneities leading to a stronger dependence of κ on v_{20}. The parameter ζ may similarly be augmented at high values of v_{20}.

Further contributions from the elastic action of entanglements on the transformation of the radius of gyration have been omitted in the present study. Such contributions were considered in the analysis of birefringence,[16,17] segmental orientation,[18,19] and local segmental mobility[25–27] of amorphous networks where the deformation tensor of the domains of constraint was denoted by Θ^2. Contributions from Θ^2 to birefringence, segmental orientation, and local segmental mobility were substantial as experimental evidence indicated. Contributions from this source to the extension of the mean-squared radius of gyration along the principal direction t is expected to be proportional to $(\bar{\Theta}_t^2 - 1)$, where $\bar{\Theta}_t^2$ in this case represents the average over all sequences of a chain. Evaluation of this average requires an integration corresponding to eq 21. Numerical calculations performed but not included in the present study show that contributions from this source to $\Lambda_{g,t}^2$ are insignificant at all levels of macroscopic strain. This observation is in agreement with SANS results. Significant contributions to $\Lambda_{g,t}$ from the elastic action of entanglements would enhance the dependence of $\Lambda_{g,\parallel}$ on macroscopic strain, in contradiction to experimental evidence.

It should be noted that for three of the four sets of data considered in this study, values of κ required for good fit to experimental data are smaller than those obtained by the use of eq 9. The discrepancy is not large, however. The final evaluation of the theory presented awaits further SANS experiments performed in conjunction with independent measurements (e.g., stress–strain experiments) of the parameter κ.

The differences between transformations of the mean-squared chain vector and radius of gyration indicated by the present study become more pronounced with increasing junction functionality. In the limit of infinite functionality, $\varphi \to \infty$, the functions B_t and $\bar{B}_t$ approach zero. Substitution into eq 13 and 25 yields, in this limit,

$$\Lambda_t^2 = \lambda_t^2 \qquad \Lambda_{t,g}^2 = (\lambda_t^2 + 1)/2 \tag{27}$$

showing that the end-to-end chain vectors transform affinely whereas the radii of gyration transform as in the phantom network.

The present treatment may be applied to the analysis of the q-dependence of scattering intensities from real networks. Calculation of the form factor for a phantom network is given by Pearson.[9] Calculations for a real network according to the constrained junction model should in principle follow the treatment of Pearson with proper identification of constraints on chain sequences. Calculation of the form factor has recently been attempted by Vilgis and Boue.[28] Improvement of their treatment by properly including the important variables v_{20}, v_2, and the constraints on sequences may lead to results that may be compared with experimental data.

Registry No. Polyisoprene, 9003-31-0; polystyrene, 9003-53-6.

References and Notes

(1) Benoit, H.; Decker, D.; Duplessix, R.; Picot, C.; Rempp, P.; Cotton, J. P.; Farnoux, B.; Jannink, G.; Ober, R. *J. Polym. Sci., Polym. Phys. Ed.* **1976**, *14*, 2119.
(2) Hinckley, J. A.; Han, C. C.; Moser, B.; Yu, H. *Macromolecules* **1978**, *11*, 836.
(3) Clough, S. B.; Maconnachie, A.; Allen, G. *Macromolecules* **1980**, *13*, 774.
(4) Beltzung, M.; Picot, C.; Rempp, P.; Herz, J. *Macromolecules* **1982**, *15*, 1594.
(5) Bastide, J.; Duplessix, R.; Picot, C.; Candau, S. *Macromolecules* **1984**, *17*, 83.
(6) Beltzung, M.; Picot, C.; Herz, J. *Macromolecules* **1984**, *17*, 663.

(7) Yu, H.; Kitano, T.; Kim, C. Y.; Amis, E. J.; Chang, T.; Landry, M.; Wesson, J. A.; Han, C. C.; Lodge, T. P.; Glinka, C. *J. Polym. Prepr.* **1985**, *26-2*, 60.
(8) Benoit, H.; Duplessix, R.; Ober, R.; Cotton, J. P.; Farnoux, B.; Jannink, G. *Macromolecules* **1975**, *8*, 451.
(9) Pearson, D. S. *Macromolecules* **1977**, *10*, 696.
(10) Warner, M.; Edwards, S. F. *J. Phys. A* **1978**, *11*, 1649.
(11) Ullman, R. *J. Chem. Phys.* **1979**, *71*, 436.
(12) Ullman, R. *Macromolecules* **1982**, *15*, 1395.
(13) Ullman, R. *Macromolecules* **1986**, *19*, 1748.
(14) Bastide, J.; Picot, C.; Candau, S. *J. Macromol. Sci., Phys.* **1981**, *B19*, 13.
(15) Ullman, R. *Macromolecules* **1982**, *15*, 582.
(16) Erman, B.; Flory, P. J. *Macromolecules* **1983**, *16*, 1601.
(17) Erman, B.; Flory, P. J. *Macromolecules* **1983**, *16*, 1607.
(18) Erman, B.; Monnerie, L. *Macromolecules* **1985**, *18*, 1985.
(19) Queslel, J. P.; Erman, B.; Monnerie, L. *Macromolecules* **1985**, *18*, 1991.
(20) Flory, P. J. *J. Chem. Phys.* **1977**, *66*, 5720.
(21) Flory, P. J.; Erman, B. *Macromolecules* **1982**, *15*, 800.
(22) Flory, P. J. *Proc. R. Soc. London, A* **1976**, *351*, 351.
(23) Erman, B.; Flory, P. J. *Macromolecules* **1982**, *15*, 806.
(24) Erman, B.; Flory, P. J. *Macromolecules* **1986**, *19*, 2342.
(25) Erman, B.; Monnerie, L. *Polym. Commun.* **1986**, *27*, 240.
(26) Erman, B.; Monnerie, L. *Macromolecules* **1986**, *19*, 2745.
(27) Jarry, J. P.; Erman, B.; Monnerie, L. *Macromolecules* **1986**, *19*, 2750.
(28) Vilgis, T.; Boue, F. *Polymer* **1986**, *27*, 1154.

Relaxation Mechanism of Polymer Melts†

André Lee and Richard P. Wool*

Department of Materials Science and Engineering, University of Illinois, 1304 W. Green St., Urbana, Illinois 61801. *Received December 15, 1986*

ABSTRACT: A centrally deuteriated triblock polystyrene was used to probe the mechanism of orientation relaxation of a step strained polymer melt. On the basis of the reptation model, the orientation of the chain should relax from the ends toward the center of the chain. Since the center block was deuteriated, the FT-IR dichroism method was ideally suited to simultaneously monitor both the orientation relaxation of the central segments and the protonated ends of the chain. The infrared results showed that the deuteriated center block loses little orientation initially and decays in a predictable exponential manner after some time. These observations strongly support the reptation model for melt dynamics. The data are discussed in terms of the fraction of the deuteriated center block remaining in the initial tube, while the entire chain executes a one-dimensional curvilinear diffusion with relaxation of entanglements.

1. Introduction

On the basis of the reptation model of polymer melts,[1-3] over a long time scale, the entire chain, on average, moves coherently back and forth along the contour of the chain and the orientation of the chain relaxes from the ends toward the center. To examine the reptation mechanism, we used a centrally deuteriated polystyrene (DPS) triblock copolymer to observe the relaxation process of deformed polymer melts. Since the infrared vibrational frequencies of the deuteriated group are different from that of the protonated group (Figure 1), the centrally deuteriated triblock copolymer has the ideal chemical structure to investigate such a relaxation mechanism.

Previously, we have used the infrared dichorism method to study both the uniaxially strained homopolymer melts[4] and matrix effects on the relaxation of labeled polymer chains.[5] The process of the orientation relaxation for a short chain in a long chain matrix was shown to be dominated by the reptation mechanism, whereas the long chain relaxation in a lower molecular weight matrix was dominated by contraint release. Therefore, the triblock copolymer was immersed in the protonated polystyrene (HPS) matrix of higher molecular weight to ensure the domination of the reptation mechanism.

The portion of the chain which escaped from its initial tube was described by the analysis of the one-dimensional random walk.[1-7] A portion of the chain was said to have relaxed its orientation when it had escaped from the initial deformed state. Thus, the measured normalized Hermans orientation function at time t is a measure of the fraction of the chain still trapped in the initial conformation at that time. Since the chain is moving back and forth at any given time, the relaxation could be assumed to be symmetrical with respect to the center of the chain; i.e., on the average, at a given time, the chain had relaxed fractions at both ends as described by the minor chain reptation model.[7]

Some recent stress–strain experiments have been done on centrally deuteriated triblock polystyrenes,[8] and the nonuniform relaxation of the chain segments has been observed at short times. The calculations[9] of the orientation function for the central and end segments have also been discussed. In this paper we focus on the dynamics of the long time relaxation processes of the central deuteriated block. In section 2, we present the calculation for the fraction and orientation of the center block remaining at time t, based on the minor chain reptation model.[7] In section 3, the experimental procedures are presented. In section 4, the results of experiment are compared with theory and discussed. The summary and conclusions are given in section 5.

2. Theoretical Considerations

Previously, the calculation of the orientation relaxation of step strained polymer melts was made by using the analysis of a one-dimensional random walk.[4] For a pure random walk, the probability of moving to the left should be the same as moving to the right. Thus, for a long enough walk, on the average, the number of steps to the left would be the same as the number of steps to the right. So, for a long chain, the orientation relaxation process is symmetrical with respect to the center of the chain. To compare with the experimental results, we made calculations using a one-third centrally labeled polymer chain (25 000 HPS–25 000 DPS–25 000 HPS), whose spectrum is shown in Figure 1.

The fraction of the chain, $F(t)$, still trapped in the initial tube at time t is given by[1]

$$F(t) = \frac{8}{\pi^2} \sum_{p=\text{odd}} \frac{1}{p^2} \exp\left(-p^2 \frac{t}{T_r}\right) \qquad (1)$$

† Presented at the Materials Research Society, Boston, Dec 1986.

0024-9297/87/2220-1924$01.50/0